

in the hypothalamic regions were determined.

To detect protein expression of  $\alpha 1$  and  $\alpha 2$  DN-AMPK and  $\gamma 1$  CA-AMPK in the hypothalamus after injection of adenoviruses, we immunoprecipitated AMPK from hypothalamic lysates (500  $\mu$ g of protein pooled from 5–6 animals) with a polyclonal antiserum recognizing the  $\alpha 1$ ,  $\alpha 2$ ,  $\beta 1$ ,  $\beta 2$  and  $\gamma 1$  subunits of AMPK (for CA-AMPK) (gift from D. Carling) or this antiserum combined with sheep  $\alpha 1$  and  $\alpha 2$  antiserum (for DN-AMPK) bound to protein-A and -G sepharose beads, and blotted with monoclonal antibodies against the c-Myc tag (for  $\alpha 1$  and  $\alpha 2$  DN-AMPK) (9B11, Cell Signalling) or the HA tag (for  $\gamma 1$  CA-AMPK) (Roche).

## Detection of mRNA of DN- and CA-AMPK

Total RNA was isolated from PVH, ARH, VMH/DMH and LH by TriReagent (Molecular Research Center). First-strand cDNA was synthesized from 2  $\mu$ g of total RNA using reverse transcriptase (Ambion) primed by random decamer. PCR amplification of Myc-tagged  $\alpha 1$  and  $\alpha 2$  DN-AMPK and HA-tagged  $\gamma 1$  CA-AMPK was performed with Platinum Taq DNA polymerase (Invitrogen). The conditions of PCR and design of the primers are described in Supplementary Methods.

## Statistical analysis

All values are mean  $\pm$  s.e.m. Data were evaluated by factorial analysis of variance and the Newman-Keuls multiple range test.

Received 22 December 2003; accepted 27 February 2004; doi:10.1038/nature02440.

Published online 17 March 2004.

- Hardie, D. G., Scott, J. W., Pan, D. A. & Hudson, E. R. Management of cellular energy by the AMP-activated protein kinase system. *FEBS Lett.* **546**, 113–120 (2003).
- Schwartz, M. W. *et al.* Central nervous system control of food intake. *Nature* **404**, 661–671 (2000).
- Friedman, J. M. & Halaas, J. L. Leptin and the regulation of body weight in mammals. *Nature* **395**, 763–770 (1998).
- Brüning, J. C. *et al.* Role of brain insulin receptor in control of body weight and reproduction. *Science* **289**, 2122–2125 (2000).
- Levin, B. E. Glucosensing neurons do more than just sense glucose. *Int. J. Obes. Relat. Metab. Disord. Suppl.* **5**, S68–S72 (2001).
- Obici, S. *et al.* Central administration of oleic acid inhibits glucose production and food intake. *Diabetes* **5**, 271–275 (2002).
- Hawley, S. A. *et al.* Complexes between the LKB1 tumor suppressor, STRADA/ $\beta$  and MO25/ $\alpha$ / $\beta$  are upstream kinases in the AMP-activated protein kinase cascade. *J. Biol.* **2**(28), 1–16 (2003).
- Turnley, A. M. *et al.* Cellular distribution and developmental expression of AMP-activated protein kinase isoforms in mouse central nervous system. *J. Neurochem.* **72**, 1707–1716 (1999).
- Culmse, C., Monnig, J., Kemp, B. E. & Mattson, M. P. AMP-activated protein kinase is highly expressed in neurons in the developing rat brain and promotes neuronal survival following glucose deprivation. *J. Mol. Neurosci.* **17**, 45–58 (2001).
- Elmqvist, J. K., Elias, C. F. & Saper, C. B. From lesions to leptin: hypothalamic control of food intake and body weight. *Neuron* **22**, 221–232 (1999).
- Obici, S., Zhang, B. B., Karkanas, G. & Rossetti, L. Hypothalamic insulin signaling is required for inhibition of glucose production. *Nature Med.* **8**, 1376–1382 (2002).
- Ollmann, M. M. *et al.* Antagonism of central melanocortin receptors *in vitro* and *in vivo* by agouti-related protein. *Science* **278**, 135–138 (1997).
- Woods, A. *et al.* Characterization of the role of AMP-activated protein kinase in the regulation of glucose-activated gene expression using constitutively active and dominant negative forms of the kinase. *Mol. Cell. Biol.* **20**, 6704–6711 (2000).
- Viollet, B. *et al.* The AMP-activated protein kinase  $\alpha 2$  catalytic subunit controls whole-body insulin sensitivity. *J. Clin. Invest.* **111**, 91–98 (2003).
- Andersson, U. *et al.* AMP-activated protein kinase plays a role in the control of food intake. *J. Biol. Chem.* published online 23 January 2004 (doi:10.1074/jbc.C300557200).
- Bates, S. H. *et al.* STAT3 signalling is required for leptin regulation of energy balance but not reproduction. *Nature* **421**, 856–859 (2003).
- Niswender, K. D. *et al.* Intracellular signalling. Key enzyme in leptin-induced anorexia. *Nature* **413**, 794–795 (2001).
- Zhao, A.-Z. *et al.* A phosphatidylinositol 3-kinase-phosphodiesterase 3B-cyclic AMP in hypothalamic action of leptin on feeding. *Nature Neurosci.* **5**, 727–728 (2002).
- Obici, S. *et al.* Inhibition of hypothalamic carnitine palmitoyltransferase-1 decreases food intake and glucose production. *Nature Med.* **9**, 756–761 (2003).
- Cowley, M. A. *et al.* Integration of NPY, AGRP, and melanocortin signals in the hypothalamic paraventricular nucleus: evidence of a cellular basis for the adipostat. *Neuron* **24**, 155–163 (1999).
- Light, P. E., Wallace, C. H. R. & Dyck, J. R. B. Constitutively active adenosine monophosphate-activated protein kinase regulates voltage-gated sodium channels. *Circulation* **107**, 1962–1965 (2003).
- Hallows, K. R. *et al.* Inhibition of cystic fibrosis transmembrane conductance regulator by novel interaction with the metabolic sensor AMP-activated protein kinase. *J. Clin. Invest.* **12**, 1711–1721 (2000).
- da Silva Xavier, G. *et al.* Role for AMP-activated protein kinase in glucose-stimulated insulin secretion and preproinsulin gene expression. *Biochem. J.* **371**, 761–774 (2003).
- Spanswick, D. *et al.* Leptin inhibits hypothalamic neurons by activation of ATP-sensitive potassium channels. *Nature* **390**, 521–525 (1997).
- Spanswick, D. *et al.* Insulin activates ATP-sensitive  $K^+$  channels in hypothalamic neurons of lean, but not obese rats. *Nature Neurosci.* **3**, 757–758 (2000).
- Loftus, T. M. *et al.* Reduced food intake and body weight in mice treated with fatty acid synthase inhibitors. *Science* **288**, 2379–2381 (2000).
- Hu, Z., Cha, S. H., Chohann, S. & Lane, D. Hypothalamic malonyl-CoA as a mediator of feeding behavior. *Proc. Natl Acad. Sci. USA* **100**, 12624–12629 (2003).
- Ruderman, N. B., Saha, A. K., Vavvas, E. & Witters, L. A. Malonyl-CoA, fuel sensing, and insulin resistance. *Am. J. Physiol.* **276**, E1–E18 (1999).
- Minokoshi, Y. *et al.* Leptin stimulates fatty-acid oxidation by activating AMP-activated protein kinase. *Nature* **415**, 339–343 (2002).

- Woods, S. *et al.* The  $\alpha 1$  and  $\alpha 2$  isoforms of the AMP-activated protein kinase have similar activities in rat liver but exhibit differences in substrate specificity *in vitro*. *FEBS Lett.* **397**, 347–351 (1996).
- Hayashi, T. *et al.* Metabolic stress and altered glucose transport. Activation of AMP-activated protein kinase as a unifying coupling mechanism. *Diabetes* **49**, 527–531 (2000).

Supplementary Information accompanies the paper on [www.nature.com/nature](http://www.nature.com/nature).

**Acknowledgements** We thank D. Carling for reagents and advice, J. K. Elmquist and B. B. Lowell for discussions and providing MC4R-KO mice, and C. J. Aschkenasi, C.-Y. Zhang, O. Boss, J. Yu and N. Balthasar for MC4R-KO mice. This work was supported by NIH grants (B.B.K. and M.J.B.), an EASD-ADA and Bettencourt-Schueller Foundation Fellowship (T.A.), AMPDIAMET (P.F.) and the American Diabetes Association (B.B.K. and Y.B.K.).

**Competing interests statement** The authors declare that they have no competing financial interests.

**Correspondence** and requests for materials should be addressed to B.B.K. (bkahn@bidmc.harvard.edu).

## From molecular noise to behavioural variability in a single bacterium

Ekaterina Korobkova<sup>1\*</sup>, Thierry Emonet<sup>1\*</sup>, Jose M. G. Vilar<sup>2,†</sup>, Thomas S. Shimizu<sup>3,†</sup> & Philippe Cluzel<sup>1</sup>

<sup>1</sup>The Institute for Biophysical Dynamics and the James Franck Institute, The University of Chicago, 5640 South Ellis Avenue, Chicago, Illinois 60637, USA  
<sup>2</sup>The Rockefeller University, Box 34, 1230 York Avenue, New York, New York 10021, USA

<sup>3</sup>Laboratory for Bioinformatics, Institute for Advanced Biosciences, Keio University Fujisawa, 252-8520, Japan

\* These authors contributed equally to this work

† Present addresses: Computational Biology Center, Memorial Sloan-Kettering Cancer Center, 307 East 63rd Street, New York, New York 10021, USA (J.M.G.V.); Department of Molecular and Cellular Biology, Harvard University, 16 Divinity Avenue, Cambridge, Massachusetts 02138, USA (T.S.S.)

The chemotaxis network that governs the motion of *Escherichia coli* has long been studied to gain a general understanding of signal transduction. Although this pathway is composed of just a few components, it exhibits some essential characteristics of biological complexity, such as adaptation and response to environmental signals<sup>1</sup>. In studying intracellular networks, most experiments and mathematical models<sup>2–5</sup> have assumed that network properties can be inferred from population measurements. However, this approach masks underlying temporal fluctuations of intracellular signalling events. We have inferred fundamental properties of the chemotaxis network from a noise analysis of behavioural variations in individual bacteria. Here we show that certain properties established by population measurements, such as adapted states, are not conserved at the single-cell level: for timescales ranging from seconds to several minutes, the behaviour of non-stimulated cells exhibit temporal variations much larger than the expected statistical fluctuations. We find that the signalling network itself causes this noise and identify the molecular events that produce it. Small changes in the concentration of one key network component suppress temporal behavioural variability, suggesting that such variability is a selected property of this adaptive system.

At the level of populations, it is well-established that the chemotaxis network produces a steady output in the absence of external stimuli, generally referred to as 'adapted steady-states'. This mechanism<sup>3</sup> allows bacteria to maintain their steady-state behaviour independently of the absolute concentration of chemo-effectors in their environment<sup>5</sup>. Because the network's output from individual cells is noisy (that is, it fluctuates randomly), it is standard practice

to average responses across a population of cells, which eliminates part of the information required to understand how an individual cell performs basic computations<sup>6,7</sup>. But noise is not always a nuisance: it can carry important information about intracellular signalling events<sup>8–10</sup>. We investigated how the behaviour of an individual bacterium of *E. coli* in a homogeneous environment fluctuates with time. In particular, we asked whether there are specific molecular events that could cause temporal behavioural variability in an individual cell.

We monitored the switching events of individual flagellar motors<sup>11</sup> from non-stimulated cells in a medium in which attractant was not present. Bacteria were immobilized onto microscope slides and flagella were marked with micro-beads to visualize their rotation with dark-field illumination<sup>12</sup>. Binary time series constructed from the clockwise (CW) and the counterclockwise (CCW) rotations of a single motor defined the chemotaxis network output<sup>11</sup> (Fig. 1a). The CW bias is the fraction of time that a motor spends rotating in the CW direction<sup>11,13</sup> (Fig. 1b). We studied the temporal variations of the CW bias by carrying out spectral analysis of the binary time series generated by switching events of individual bacterial motors. In this approach, the power spectrum is a measure of the amplitude of the fluctuations of the CW bias at a given timescale. The standard assumption has been that switching events are independent and governed by a Poisson process, which implies that the CW and CCW time intervals are uncorrelated and exponentially distributed<sup>13</sup>. Under these assumptions, the power spectrum would exhibit a flat profile over timescales larger than the typical switching time (Supplementary Information).

We recorded a 170-min-long time series of switching events from an individual motor of a RP437 wild-type bacterium, which was immersed in a medium in which no attractant was present and that did not support growth. Unexpectedly, the corresponding power spectrum exhibited a growing profile up to 15 min ( $\sim 10^3$  s, Fig. 2a). The fact that the power spectrum is not flat indicates that the CCW and CW intervals are either not ‘independently and identically distributed (IID)’, or IID but not exponentially distributed. It also means that the variability of the CW bias over these timescales is larger than that expected from a motor with exponentially distributed intervals and similar mean switching frequency. Because not all the cells exhibited the same temporal variability, the slopes of power spectra varied from cell to cell, but all fell into the open interval (0, 1). Consequently, we computed 222 power spectra from clonal individual RP437 wild-type cells and summarized their average trend in Fig. 2b. We found that the trend of 222 individual

power spectra exhibited a growing profile as frequencies decreased. The temporal variability of the network output, the CW bias, was larger than that expected from uncorrelated and exponentially distributed CW and CCW intervals<sup>14,15</sup>.

To reconcile our data with ensemble measurements, we averaged together the previous 222 binary time series from individual cells before spectral analysis so that we could study the nature of the fluctuations of the bias of a population. The resulting power spectrum exhibited a flat profile at any timescale greater than seconds, indicating that the temporal variations of the bias obtained from a population could be produced by uncorrelated, exponentially distributed CW and CCW intervals<sup>13</sup> (Fig. 2b, inset). In this system, the time average of single-cell behaviour differs from population behaviour for timescales ranging from few to  $10^3$  seconds.

The chemotaxis network is a phosphoryl cascade that controls the concentration of the phosphorylated form of a signalling molecule, the soluble response regulator CheY<sup>1</sup> (Supplementary Information). The phosphorylated form, CheY-P, binds preferentially to the cytoplasmic base of the motors. When the concentration of CheY-P increases, motors spend more time spinning clockwise. To investigate the molecular origin of behavioural variability of single PS2001 mutant cells, we used the activated CheYD13K mutant, which mimics the effect of CheY-P but does not need to be phosphorylated to be active<sup>4</sup>. The active CheYD13K signalling molecule was expressed so that the mean CW bias from the population would be at about the wild-type level. The power spectrum associated with the CheYD13K mutant provided the spectral characteristics of the bacterial motor (Fig. 2b). At short timescales the spectrum was similar to wild type and peaked at about one second. For longer timescales, the data showed that when the concentration of the active form of the signalling molecule was not regulated by the chemotaxis network, but stably expressed from an inducible plasmid, the noise level was much lower than in wild-type cells (Fig. 2b). This result suggests that temporal behavioural variability in a wild-type cell emerges from the signalling processes taking place in the network itself.

We characterized the underlying statistical nature of the distributions of the CW and CCW switching events in the PS2001 mutant and wild-type cells. An individual wild-type cell exhibits a distribution of short CW length intervals that is dominated by an exponential behaviour (Fig. 2c). However, we found that the distribution of CCW intervals from several wild-type cells deviates significantly from exponential behaviour<sup>14,16</sup> (Fig. 2c). In particular, this distribution could instead be approximated at long timescales

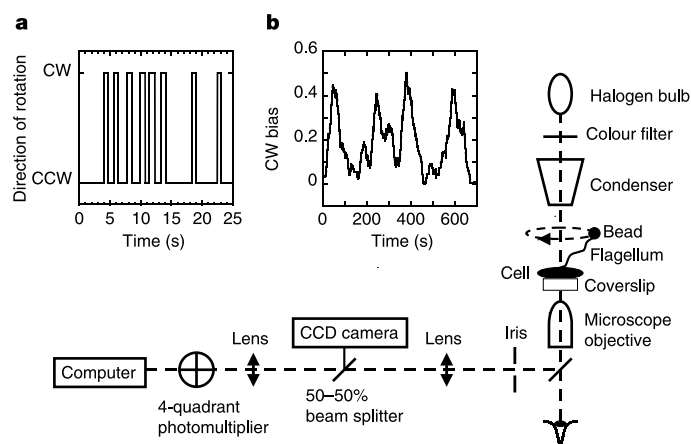


**Figure 1** Schematic view of the apparatus. Cells were specifically attached onto a microscope slide. Latex beads (0.5  $\mu\text{m}$ , Polysciences) were used as markers to visualize single rotating flagella<sup>12</sup> on an inverted microscope with dark-field illumination. A four-quadrant photomultiplier (PMT) was used to record the trajectory of the bead. Typical

assays lasted from 10 to 20 min. **a**, Binary time series, indicating the direction of rotation. **b**, CW bias versus time. The bias was computed as the fraction of time the bead span clockwise within a 30 s moving window.

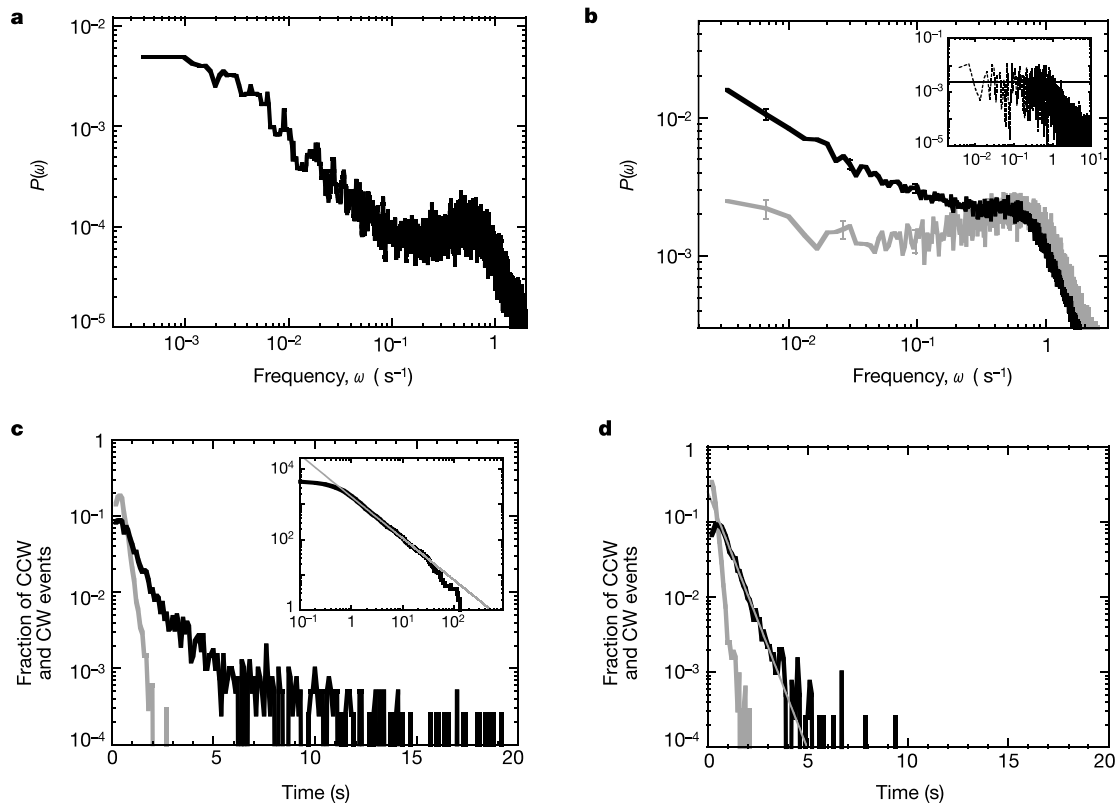


**Figure 2** Noise of the chemotaxis network. **a**, Power spectrum of the network output from one non-stimulated individual wild-type cell. **b**, Mean spectrum computed by averaging the spectra from wild-type and mutant cells. Black line, mean spectrum from 40 wild-type cells; grey line, spectral characteristics of the bacterial motor. Mean power spectrum of individual power spectra from 16 PS2001 mutant cells complemented by the inducible *cheYD13K* gene ([IPTG] = 25, 30  $\mu$ M). The error bars (grey and black line) show the

standard error. Inset, power spectrum of the CW bias of a population of 40 cells.

**c**, Distribution of CW (grey) and CCW (black) intervals from the cell in **a**. Inset, cumulative distribution of the same CCW intervals (black line). Power law with an exponent of approximately  $-1.2$  (grey straight line). **d**, CW and CCW interval distributions from eight mutants (PS2001) expressing *CheYD13K* (CW bias ranging from 0.2 to 0.3).

by a power law (Fig. 2c, inset). For mutant cells in which the motor output was decoupled from the activity of the signalling pathway, both CW and CCW intervals were exponentially distributed (Fig. 2d).

To determine the specific molecular events that account for the observed temporal variability of the CW bias, we focused on receptor methylation (Supplementary Information), which has been shown through population measurements to be a key determinant of the steady-state motor bias<sup>3,5,17</sup>. We investigated how the temporal behavioural variability noted above depends on the concentration of the methyltransferase CheR, which adds methyl groups at multiple receptor residues. The *cheR*-deleted RP4968 mutant was complemented with a *lac*-inducible low-copy plasmid expressing the CheR protein<sup>5</sup>. Intracellular concentration, [CheR], was varied over an approximately tenfold range by induction with increasing amounts of isopropyl- $\beta$ -D-thiogalactoside, [IPTG] (Methods). At low [CheR] ([IPTG] = 0  $\mu$ M), wild-type levels of behavioural variability were recovered. At timescales greater than seconds, the power spectrum of the network output of individual cells exhibited a growing profile similar to that of wild-type cells (Fig. 3a). Surprisingly, as [CheR] was increased to about two times the wild-type concentration ([IPTG] = 1  $\mu$ M), the power spectrum exhibited a weaker slope, which faded away for values of [CheR]  $\geq$  four times the wild-type level (Fig. 3a). Similarly, as [CheR] was increased, the initially power-law-distributed CCW intervals segued towards exponential behaviour (Fig. 3b). Therefore, the temporal behavioural variability could be reduced and furthermore suppressed by increasing [CheR]. For individual wild-type cells with low [CheR], the output bias exhibited temporal variations

greater than statistical fluctuations expected from an exponential distribution of uncorrelated CW and CCW intervals, whereas for slightly higher [CheR] this noise was markedly suppressed (Fig. 3c).

To gain further insights into the signalling pathway, we simulated the chemical reactions between the cytosolic chemotaxis proteins (CheR, CheB, CheY and CheZ) and the receptor-kinase complexes (Supplementary Information). To capture time correlations in a reacting system, we performed stochastic simulations using the StochSim package<sup>6</sup> (Methods). We simulated the temporal fluctuations in CheY-P concentration and computed the corresponding power spectra for various values of [CheR]. For approximately wild-type levels of [CheR], the wild-type-like spectrum was qualitatively recovered (Fig. 4a). The fluctuations of concentration of the active signalling molecules (CheY-P) exhibit a strong correlated noise. Moreover, the amplitude of these fluctuations could be modulated by the methylation and demethylation of the receptors catalysed by CheR and CheB (Supplementary Information). Because CheR works at saturation, the number of active receptors increases nonlinearly in an ultra-sensitive<sup>19,20</sup> fashion with [CheR] (data not shown). At wild-type concentrations of CheR, about half of the receptors are active and the associated fluctuations of [CheY-P] are maximal<sup>21,22</sup>. For higher [CheR], four times the wild-type level or more, almost all the receptors are active and the associated fluctuations of [CheY-P] are smaller (Fig. 4b).

To support the hypothesis that the methylation process controls temporal behavioural variability, we analysed the noise from the RP8610 (RP8610 strain and pRR27 plasmid; J. S. Parkinson, personal communication) mutant deleted for the *cheR*, *cheB* and all

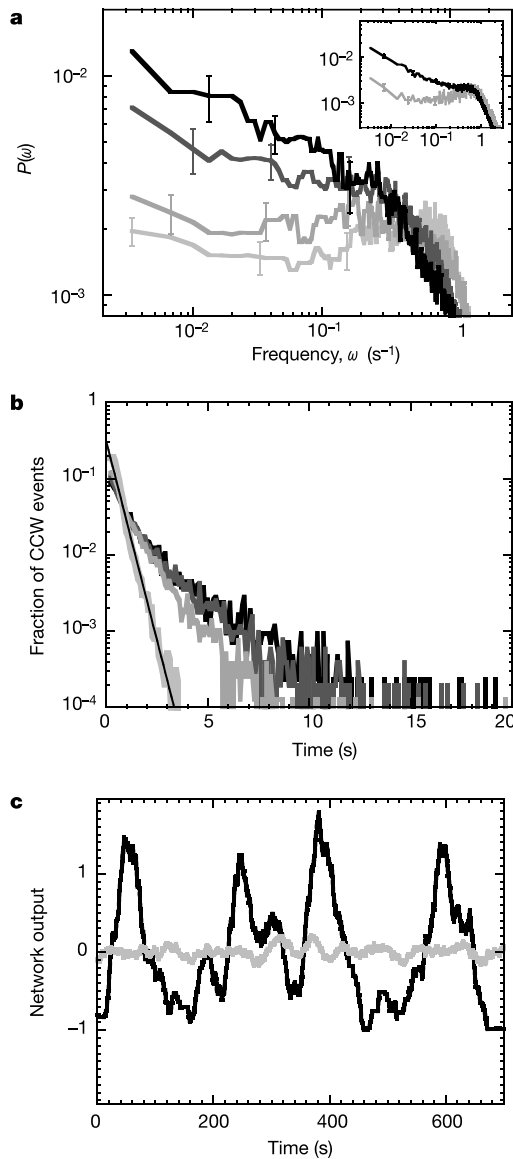


**Figure 3** Behavioural variability as a function of [CheR]. **a**, Average power spectra of the motors, switching events from RP4968 cells versus [CheR] levels. Black, wild-type level of CheR ([IPTG] = 0 μM); dark grey, twofold wild-type level ([IPTG] = 1 μM); grey, fourfold wild-type level ([IPTG] = 5 μM); light grey, tenfold wild-type level ([IPTG] = 30 μM). Error bars show the standard error. Inset, effect of fixed methylation level on behavioural variability; black, as in Fig. 2a; grey, spectra from RP 8610 mutant cells complemented with Tsr mutant serine receptors. **b**, CCW interval distributions versus [CheR] (same cells and conditions as in panel **a**). Exponential fit (straight black line). **c**, Network output signals from a wild-type and a mutant cell. Black, wild-type cell with a mean CW bias of 0.2 and a switching frequency of 0.4 s<sup>-1</sup> (same cell as in Fig. 2a); grey, RP4968 mutant (concentration ten times the wild-type level) with a mean CW bias of 0.4 and a switching frequency of 0.9 s<sup>-1</sup> (same cell as **a**; light grey). The network output is defined as [bias - < bias > ] / < bias > .

chemoreceptor genes. In this strain, mutant serine receptors that mimic the activity of receptors with a fixed level of methylation were stably expressed from a *lac*-inducible vector (Methods). The resulting variability was found to be smaller than in wild-type cells and the associated power spectra were identical to the spectral characteristics of the motor when uncoupled from the network (Fig. 3a, inset; compare with Fig. 2b). This result suggests that the slow methylation process of the receptors contributes to the observed behavioural variability.

It is conceivable that such variability, and in particular the power-

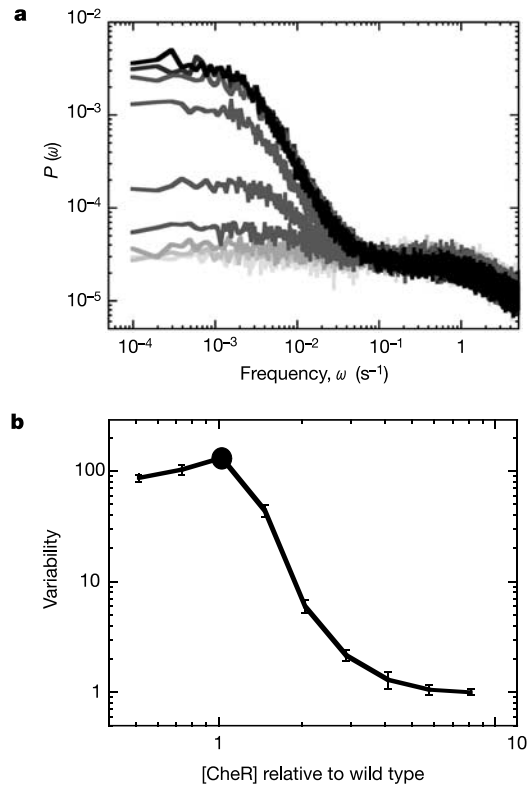


**Figure 4** Simulated variability of the chemotaxis network. **a**, Power spectra of simulated temporal variations of the signalling molecule concentration [CheYp] for increasing [CheR]. [CheR] was increased from 0.5 (black) to eight times the wild-type level (light grey). In the frequency interval 0.1–1 Hz, the spectra displayed a flat region robust to changes in [CheR]. **b**, Variability of the network output [CheYp] versus [CheR]. Wild-type cell as in ref. 6 (filled circle). The variability was defined as the power of the output signal (for a chosen [CheR]) normalized by the power of the network output for a [CheR] eight times the wild-type level. Means of the power and standard deviations were computed for a frequency interval (10<sup>-3</sup>, 10<sup>-4</sup> Hz).

law behaviour of CCW intervals, will be reflected in the run-length distribution of individual swimming cells. A power-law distribution of the run lengths may provide bacteria with an optimal search strategy to adapt to a complex environment with a sparse distribution of nutrients<sup>23</sup> (Supplementary Information).

Three decades ago, Spudich and Koshland established the existence of ‘non-genetic individuality’ in clonal populations of *Salmonella typhimurium*<sup>24</sup>. We analysed the molecular origin of the temporal variations in signalling within individual bacteria. Both experimental and simulation data showed that within individual bacteria, molecular noise emerges as a tunable source of behavioural variability (Figs 3c and 4b). If the relative concentration of a key chemotaxis protein ([CheR]) had been slightly higher, any wild-type cell would have exhibited a steadier behaviour. Our results revealed that such a regime was not selected for in the chemotaxis system. On the contrary, the presence of a large temporal behavioural variability in this simple sensory system<sup>19,21,22</sup> appears to be the manifestation of the ‘adapted’ state of wild-type cells (Fig. 4b). Considering the ubiquity in nature of signalling pathways with similar design principles<sup>19</sup>, it would be surprising not to find that molecular noise in other signal transduction networks is also a selectable source of cell fate variability. □

**Methods**

**Bacterial strains and plasmids**

Cells were grown from an overnight culture in tryptone broth at 30 °C and then harvested (optical density = 0.5 at 595 nm). Cells were then washed and suspended in minimal

medium (7.6 mM (NH<sub>4</sub>)<sub>2</sub>SO<sub>4</sub>, 2 mM MgSO<sub>4</sub>, 20 μM FeSO<sub>4</sub>, 0.1 mM EDTA, 0.1 mM L-methionine, 60 mM potassium phosphate pH 6.8). PS2001 and DeltaR RP4968 mutants were grown with various IPTG concentrations. CheYD13K was expressed from pMS164 (ref. 5). The average [CheR] (expressed from pUA4) was estimated using the relationship between [IPTG] and [CheR] assessed by immunoblots in ref. 5.

## PS2001 strain

This strain is deleted for *CheB*, *CheZ* and *CheY*. The strain was transformed with an inducible *lac* promoter pMS164 (ref. 4) plasmid expressing a *cheYD13K* gene. The CheYD13K mutant acts like CheY-P but does not need to be phosphorylated to be active. The active CheYD13K signalling molecule was expressed from the *lac*-inducible vector pMS164 (with [IPTG] = 25–30 μM).

## RP4968 strain

*cheR* is deleted in this strain. Cells were complemented with a *lac*-inducible low-copy plasmid pUA4 (ref. 5) expressing the CheR protein. CW bias was controlled by the induction level of CheR.

## RP8610 strain

This strain carries a complete deletion of *cheR*, *cheB*, *tsr*, *tar*, *tap* and *trg*. The strain was transformed with an inducible *lac* promoter pRR27 plasmid expressing the *Tsr* mutant gene<sup>20</sup>. The methylation sites of this *Tsr* mutant are QQQQE. Varying the *Tsr* expression allowed us to set the steady-state bias at any value. In Fig. 3a (inset), the bias was adjusted to about wild-type level.

## Simulations

The reaction system was based on a two-state model<sup>18</sup> of receptor activation, and its parameter values used to simulate the wild-type behaviour were identical to those described in ref. 6. In Fig. 4, [CheR] was incremented from its wild-type value in factors of  $\sqrt{2}$ . For each value of [CheR], 63 independent time sequences of CheYp (each 170 min long) were generated and normalized by their standard deviation. The average of the 63 corresponding power spectra was plotted for each [CheR].

Received 30 August 2003; accepted 5 February 2004; doi:10.1038/nature02404.

- Bouret, R. B. & Stock, A. M. Molecular information processing: lessons from bacterial chemotaxis. *J. Biol. Chem.* **277**, 9625–9628 (2002).
- Spiro, P. A., Parkinson, J. S. & Othmer, H. G. A model of excitation and adaptation in bacterial chemotaxis. *Proc. Natl Acad. Sci. USA* **94**, 7263–7268 (1997).
- Barkai, N. & Leibler, S. Robustness in simple biochemical networks. *Nature* **387**, 913–917 (1997).
- Alon, U. *et al.* Response regulator output in bacterial chemotaxis. *EMBO J.* **17**, 4238–4248 (1998).
- Alon, U., Surette, M. G., Barkai, N. & Leibler, S. Robustness in bacterial chemotaxis. *Nature* **397**, 168–171 (1999).
- Morton-Firth, C. J., Shimizu, T. S. & Bray, D. A free-energy-based stochastic simulation of the Tar receptor complex. *J. Mol. Biol.* **286**, 1059–1074 (1999).
- Morton-Firth, C. J. & Bray, D. Predicting temporal fluctuations in an intracellular signalling pathway. *J. Theor. Biol.* **192**, 117–128 (1998).
- Katz, B. & Miledi, R. Statistical nature of acetylcholine potential and its molecular components. *J. Physiol. (Lond.)* **224**, 665–699 (1972).
- Samuel, A. D. & Berg, H. C. Fluctuation analysis of rotational speeds of the bacterial flagellar motor. *Proc. Natl Acad. Sci. USA* **92**, 3502–3506 (1995).
- Rao, C. V., Wolf, D. M. & Arkin, A. P. Control, exploitation and tolerance of intracellular noise. *Nature* **420**, 231–237 (2002).
- Larsen, S. H., Reader, R. W., Kort, E. N., Tso, W. W. & Adler, J. Change in direction of flagellar rotation is the basis of the chemotactic response in *Escherichia coli*. *Nature* **249**, 74–77 (1974).
- Cluzel, P., Surette, M. & Leibler, S. An ultrasensitive bacterial motor revealed by monitoring signaling proteins in single cells. *Science* **287**, 1652–1655 (2000).
- Block, S. M., Segall, J. E. & Berg, H. C. Adaptation kinetics in bacterial chemotaxis. *J. Bacteriol.* **154**, 312–323 (1983).
- Ishihara, A., Segall, J. E., Block, S. M. & Berg, H. C. Coordination of flagella on filamentous cells of *Escherichia coli*. *J. Bacteriol.* **155**, 228–237 (1983).
- Khan, S. & Macnab, R. M. The steady-state counterclockwise/clockwise ratio of bacterial flagellar motors is regulated by protonmotive force. *J. Mol. Biol.* **138**, 563–597 (1980).
- Fahner, K. A. *Studies of Bacterial Flagellar Motors and Filaments*. PhD thesis, Harvard Univ. (1995).
- Yi, T. M., Huang, Y., Simon, M. I. & Doyle, J. Robust perfect adaptation in bacterial chemotaxis through integral feedback control. *Proc. Natl Acad. Sci. USA* **97**, 4649–4653 (2000).
- Asakura, S. & Honda, H. Two-state model for bacterial chemoreceptor proteins. The role of multiple methylation. *J. Mol. Biol.* **176**, 349–367 (1984).
- Goldbeter, A. & Koshland, D. E. Jr An amplified sensitivity arising from covalent modification in biological systems. *Proc. Natl Acad. Sci. USA* **78**, 6840–6844 (1981).
- Levit, M. N. & Stock, J. B. Receptor methylation controls the magnitude of stimulus-response coupling in bacterial chemotaxis. *J. Biol. Chem.* **277**, 36760–36765 (2002).
- Detwiler, P. B., Ramanathan, S., Sengupta, A. & Shraiman, B. I. Engineering aspects of enzymatic signal transduction: photoreceptors in the retina. *Biophys. J.* **79**, 2801–2817 (2000).
- Elf, J., Paulsson, J., Berg, O. G. & Ehrenberg, M. Near-critical phenomena in intracellular metabolite pools. *Biophys. J.* **84**, 154–170 (2003).
- Viswanathan, G. M. *et al.* Optimizing the success of random searches. *Nature* **401**, 911–914 (1999).
- Spudich, J. L. & Koshland, D. E. Jr Non-genetic individuality: chance in the single cell. *Nature* **262**, 467–471 (1976).

Supplementary Information accompanies the paper on [www.nature.com/nature](http://www.nature.com/nature).

**Acknowledgements** P.C. is indebted to S. Leibler in whose laboratory at Princeton University this work was begun. The authors thank J. Doyle for pointing out the existence of the power law in the CCW intervals distributions, H. Park for technical help with Labview software, U. Alon for sharing the expression vector pUA4, J. S. Parkinson for the RP8610 strain and the pRR27 vector, and F. Cattaneo for the use of computers. The authors are thankful to R. Albert, C. Guet, T. Griggs, C. Macal, M. North and R. Rosner for discussions and comments on the manuscript. This work was supported partially by the MRSEC programme of the NSF and the Cancer Research Foundation. T.E. acknowledges support from a joint research funding from the US Department of Energy. T.S.S. acknowledges support from NEDO, Ministry of Economy, Trade and Industry of Japan.

**Competing interests statement** The authors declare that they have no competing financial interests.

**Correspondence** and requests for materials should be addressed to P.C. (cluzel@uchicago.edu).

## The myosin motor in muscle generates a smaller and slower working stroke at higher load

Massimo Reconditi<sup>1</sup>, Marco Linari<sup>1</sup>, Leonardo Lucii<sup>1</sup>, Alex Stewart<sup>2</sup>, Yin-Biao Sun<sup>3</sup>, Peter Boesecke<sup>4</sup>, Theyencheri Narayanan<sup>4</sup>, Robert F. Fischetti<sup>5</sup>, Tom Irving<sup>5</sup>, Gabriella Piazzesi<sup>1</sup>, Malcolm Irving<sup>3</sup> & Vincenzo Lombardi<sup>1</sup>

<sup>1</sup>Laboratorio di Fisiologia, DBAG, Università di Firenze, I-50134 Firenze, and OGG, Istituto Nazionale di Fisica della Materia, Italy

<sup>2</sup>Rosenstiel Center, Brandeis University, Waltham, Massachusetts 02545, USA

<sup>3</sup>Randall Division of Cell and Molecular Biophysics, King's College London, London SE1 1UL, UK

<sup>4</sup>European Synchrotron Radiation Facility, F-38043 Grenoble Cedex, France

<sup>5</sup>BioCAT Advanced Photon Source, Argonne, Illinois 60439, USA

Muscle contraction is driven by the motor protein myosin II, which binds transiently to an actin filament, generates a unitary filament displacement or 'working stroke', then detaches and repeats the cycle. The stroke size has been measured previously using isolated myosin II molecules at low load, with rather variable results<sup>1–4</sup>, but not at the higher loads that the motor works against during muscle contraction. Here we used a novel X-ray-interference technique<sup>5,6</sup> to measure the working stroke of myosin II at constant load<sup>7</sup> in an intact muscle cell, preserving the native structure and function of the motor. We show that the stroke is smaller and slower at higher load. The stroke size at low load is likely to be set by a structural limit<sup>8,9</sup>; at higher loads, the motor detaches from actin before reaching this limit. The load dependence of the myosin II stroke is the primary molecular determinant of the mechanical performance and efficiency of skeletal muscle.

Muscle cells from skeletal and cardiac muscle are composed of many identical functional units called sarcomeres, each of which contains overlapping myosin and actin filaments (Fig. 1a). Muscle shortening is generated by the relative sliding of the two types of filament, driven by the working stroke in the myosin-head domains (Fig. 1b, c). The myosin filament (blue in Fig. 1) is symmetrical about its midpoint and contains two regular arrays of myosin heads (red in Fig. 1). When a muscle fibre is illuminated by a parallel beam of X-rays, the 14.5 nm spacing of the heads in each array produces a strong X-ray reflection called the M3. Interference between the diffracted X-rays from the two head arrays in each filament produces a finely spaced modulation of this reflection, from which the interference distance (ID; Fig. 1) between the two arrays can be measured with a precision of a few angstroms<sup>5,6</sup>. In principle, the myosin II stroke size in the intact muscle fibre can be determined